Controlling chaos in high dimensions: Theory and experiment

Mingzhou Ding and Weiming Yang
Program in Complex Systems and Brain Sciences, Center for Complex Systems and Department of Mathematics, Florida Atlantic University, Boca Raton, Florida 33431

Visarath In and William L. Ditto
Applied Chaos Laboratory, School of Physics, Georgia Institute of Technology, Atlanta, Georgia 30332

Mark L. Spano and Bruce Gluckman
Naval Surface Warfare Center, Carderock Division, Silver Spring, Maryland 20903
(Received 27 November 1995)

The main contribution of this work is the development of a high-dimensional chaos control method that is effective, robust against noise, and easy to implement in experiment. Assuming no knowledge of the model equations, the method achieves control by stabilizing a desired unstable periodic orbit with any number of unstable directions, using small time-dependent perturbations of a single system parameter. Specifically, our major results are as follows. First, we derive explicit control laws for time series produced by discrete maps. Second, we show how to apply this control law to continuous-time problems by introducing straightforward ways to extract from a continuous-time series a discrete time series that measures the dynamics of some Poincaré map of the original system. Third, we illustrate our approach with two examples of high-dimensional ordinary differential equations, one autonomous and the other periodically driven. Fourth, we present the result on our successful control of chaos in a high-dimensional experimental system, demonstrating the viability of the method in practical applications.

PACS number(s): 05.45.+b

I. INTRODUCTION

Chaotic phenomena arise ubiquitously in natural systems and in man-made devices [1]. Past work has focused mainly on the discovery and characterization of chaotic behavior occurring in situations where there is no goal-oriented intervention. Recently, ideas and techniques have been proposed to convert chaotic orbits to desired periodic ones by using temporally programmed small controls [2–9]. It is suggested that by doing so one improves the system's performance against some general classes of criteria [10]. This direction of research opens the possibility of utilizing the rich properties of chaos in practical applications and has thus attracted a great deal of interest. In the present paper we consider this chaos control paradigm in systems where the equations of motion are not known and the dynamical information is contained in a time series obtained from observing a single scalar function of the original phase space variables. Our main results are as follows.

(i) Assuming that the time series is produced by a discrete map we develop a high-dimensional chaos control method based on ideas proposed by So and Ott [7]. Here we use map-generated time series to ensure that the coefficients needed for the implementation of control are easy to estimate from experimental data. In addition, the expression of the control law involves only the knowledge about the unstable directions of the to-be-stabilized periodic orbit. This is an added practical benefit since such knowledge is often more reliably obtained from time series. It is also worth emphasizing that in this method one only needs to vary a single external parameter to control a system of arbitrary dimensionality with an arbitrary number of unstable directions.

(ii) We show that for a continuous-time system, as would be encountered in most experimental problems, simple methods can be used to extract from the continuous-time series a discrete-time series that probes the dynamics of some Poincaré map in the original phase space. Specifically, for an autonomous system, this is done by measuring the times between successive crossings of some predetermined threshold by the continuous-time series. We call these times interspike intervals. For a periodically driven system, either the interspike intervals or the more traditional stroboscopic samples can be used to form the discrete time series. In this fashion the explicit control law mentioned in (i) applies directly to continuous-time systems. Other advantages of basing the control method on discrete-time series generated by Poincaré maps are also discussed.

(iii) We illustrate our approach with two examples of ordinary differential equations, one an autonomous chemical reaction model of four variables and the other a pair of coupled Duffing oscillators with periodic forcing, a five-dimensional system. In the second example, the periodic orbit to be stabilized has two unstable directions, and in the second example, we consider the control of a period-2 orbit.

(iv) We have applied the control method to a physical system of a magnetoelastic ribbon driven by a sinusoidally varying magnetic field. We have successfully achieved the control of high-dimensional chaos where other techniques have failed to do so. We have also demonstrated the robustness of the method by showing that it works effectively in the presence of rather substantial random noise.

The rest of this paper is organized as follows. In Sec. II

we present the method of chaos control. Here we leave some of the detailed calculations to the Appendix. Section III shows how to extract a Poincaré-map-generated discrete-time series from a continuous-time system. We also discuss numerical results in this section. In Sec. IV we present the control results for the magnetoelastic ribbon experiment. We summarize the paper in Sec. V.

II. THE CONTROL METHOD

A. Delay coordinates

Consider a k-dimensional map

$$\mathbf{X}_{n+1}=\mathbf{F}(\mathbf{X}_n,p), \tag{1}$$

where $\mathbf{X}\in\mathbb{R}^k$ and p is the chosen control parameter. Suppose that for $p=\overline{p}$ Eq. (1) exhibits a chaotic attractor. Let the scalar observation function be $x=h(\mathbf{X})$. Assuming no *a priori* knowledge of the equations of motion $\mathbf{F}$, we carry out the system analysis and control by using the time series

$$\{x_n\}=\{h(\mathbf{X}_n)\}, \tag{2}$$

where $n=1,2,3,\ldots$. (In Sec. III we shall describe ways to extract such discrete-time series for both autonomous and periodically driven *continuous-time* systems.) Employing delay coordinates [11], we reconstruct the high-dimensional dynamics from $\{x_n\}$ via

$$\mathbf{z}_n=\begin{pmatrix} z_n^{(1)} \\ z_n^{(2)} \\ \vdots \\ z_n^{(m)} \end{pmatrix}=\begin{pmatrix} x_{n-m+1} \\ x_{n-m+2} \\ \vdots \\ x_n \end{pmatrix}_{m\times 1},$$

where m is the dimension of the reconstructed phase space. Results in [11] state that, for large enough m, $\mathbf{z}_n$ is a global one-to-one representation of the variable $\mathbf{X}_n$ on the original attractor. Since the application of control in this work entails that we change the value of the parameter p according to a control law at every iteration of Eq. (1), the discrete map for $\mathbf{z}_n$ is

$$\mathbf{z}_{n+1}=\mathbf{G}(\mathbf{z}_n,p_{n-m+1},p_{n-m+2},\ldots,p_n), \tag{3}$$

where $\mathbf{G}$ generally depends on all the parameter variations effective during the time interval $n-m+1\leq t\leq n$ spanned by the delay vector $\mathbf{z}_n$ [6].

Below, by taking into account of the effect of the past parameter changes specified in Eq. (3), we derive the control laws that stipulates the choice of p_n to convert the natural chaotic dynamics of Eq. (1) to a periodic orbit selected from an infinitely many contained in the chaotic attractor. The parameter variations are assumed to be small around the nominal value $p=\overline{p}$ so that no new orbits are expected to be created in the process. Thus we seek to exploit unstable periodic orbits already existing in the chaotic attractor. This control approach is also flexible in that by simply changing to a different temporal programming of the parameter p one can switch the dynamics from one periodic behavior to another without major alterations to the system.

B. Stabilizing a fixed point

We begin by considering the stabilization of a saddle fixed point that may have more than one unstable direction. In this case, the control law to be derived admits an explicit expression. Moreover, the simple setting here allows us to better illustrate the main ideas involved.

An unstable fixed point $\overline{\mathbf{X}}$ in the original chaotic attractor when $p=\overline{p}$ satisfies

$$\overline{\mathbf{X}}(\overline{p})=\mathbf{F}(\overline{\mathbf{X}}(\overline{p}),\overline{p}). \tag{4}$$

Reflected in the delay coordinate space we have

$$\overline{\mathbf{z}}(\overline{p})=\mathbf{G}(\overline{\mathbf{z}}(\overline{p}),\overline{p},\overline{p},\ldots,\overline{p}), \tag{5}$$

where $\overline{\mathbf{z}}(\overline{p})=[\overline{x(p)},\overline{x(p)},\ldots,\overline{x(p)}]^T$, T denoting matrix transpose, and $\overline{x(p)}=h(\overline{\mathbf{X}}(\overline{p}))$. The location of this fixed point can be extracted from the time series. The procedure for finding it is simplified by knowing that it lies on the diagonal in the m-dimensional reconstructed phase space.

To describe the effect of control parameter variations on the linear dynamics near the fixed point, we introduce the $m\times m$ Jacobian matrix

$$\mathbf{A}_n=\mathbf{D}_{\mathbf{z}_n}\mathbf{G}(\mathbf{z}_n,p_{n-m+1},p_{n-m+2},\ldots,p_n) \tag{6}$$

and a set of m-dimensional column vectors [7]

$$\begin{aligned}
\mathbf{B}_n^{(m)}&=D_{p_{n-m+1}}\mathbf{G}(\mathbf{z}_n,p_{n-m+1},p_{n-m+2},\ldots,p_n),\\
\mathbf{B}_n^{(m-1)}&=D_{p_{n-m+2}}\mathbf{G}(\mathbf{z}_n,p_{n-m+1},p_{n-m+2},\ldots,p_n),\\
&\vdots\\
\mathbf{B}_n^{(1)}&=D_{p_n}\mathbf{G}(\mathbf{z}_n,p_{n-m+1},p_{n-m+2},\ldots,p_n).
\end{aligned} \tag{7}$$

Evaluating all the partial derivatives at $\overline{\mathbf{z}(p)}$ and $p_{n-m+1}=p_{n-m+2}=\cdots=p_n=\overline{p}$, we obtain near the fixed point

$$\begin{aligned}
\mathbf{z}_{n+1}-\overline{\mathbf{z}(p)}=\mathbf{A}(\mathbf{z}_n-\overline{\mathbf{z}(p)})+\mathbf{B}^{(m)}(p_{n-m+1}-\overline{p})+\mathbf{B}^{(m-1)}\\
\times(p_{n-m+2}-\overline{p})+\cdots+\mathbf{B}^{(1)}(p_n-\overline{p}),
\end{aligned} \tag{8}$$

where we have dropped the reference to n in $\mathbf{A}$ and $\mathbf{B}$'s since they are now constant matrix and vectors. It should be noted that, due to the nature of the discrete-time series and delay coordinates used here, Eq. (3) in component form is

$$\begin{pmatrix} z_{n+1}^{(1)} \\ z_{n+1}^{(2)} \\ \vdots \\ z_{n+1}^{(m-1)} \\ z_{n+1}^{(m)} \end{pmatrix}=\begin{pmatrix} z_n^{(2)} \\ z_n^{(3)} \\ \vdots \\ z_n^{(m)} \\ g(\mathbf{z}_n,p_{n-m+1},p_{n-m+2},\ldots,p_n) \end{pmatrix}. \tag{9}$$

Thus most of the entries in the $\mathbf{A}$ matrix and the $\mathbf{B}$ vectors are zero. Specifically,

$$\mathbf{A}=\begin{pmatrix} 0 & 1 & 0 & \cdots & 0 \\ 0 & 0 & 1 & \cdots & 0 \\ \vdots & \vdots & \vdots & \vdots & \vdots \\ 0 & 0 & 0 & \cdots & 1 \\ a^{(m)} & a^{(m-1)} & a^{(m-2)} & \cdots & a^{(1)} \end{pmatrix}_{m\times m} \tag{10}$$

and

$$\mathbf{B}^{(i)}=\begin{pmatrix} 0 \\ 0 \\ \vdots \\ 0 \\ b^{(i)} \end{pmatrix}_{m\times 1}, \tag{11}$$

where $i=1,2,\ldots,m$. The use of Poincaré-map-generated time series reduces our task of obtaining the entire $\mathbf{A}$ and $\mathbf{B}^{(i)}$ to the estimation of only $a^{(1)},a^{(2)},\ldots,a^{(m)}$, $b^{(1)},b^{(2)},\ldots,b^{(m)}$ from the experimental data. We remark that, although it is possible to obtain the values of $a^{(i)}$'s and the $b^{(i)}$'s together at the same time, our experience indicates that the best strategy is to find the $a^{(i)}$'s first based on the unperturbed time series and then to apply the perturbation to calculate the $b^{(i)}$'s. The perturbation is applied in such a way that only one δp is not zero in the time interval spanned by $\mathbf{z}_n$. See Sec. IV for more discussions on the estimation of $a^{(i)}$'s and $b^{(i)}$'s.

Assume that $\mathbf{A}$ in Eq. (10) has u unstable directions and s stable directions ($s+u=m$) with eigenvalues λ_i satisfying $|\lambda_1|>|\lambda_2|>\cdots>|\lambda_u|>1>|\lambda_{u+1}|>|\lambda_{u+2}|>\cdots>|\lambda_m|$. Let $\mathbf{e}_i$ denote the corresponding eigenvectors. Then a possible control approach is to choose suitable parameter variations according to Eq. (8) to push the trajectory $\mathbf{z}_{n+1}$ into the stable subspace spanned by the stable directions $\mathbf{e}_i$, $i=u+1,u+2,\ldots,m$. However, Dressler and Nistche [6] point out for the $m=2$ case that this strategy may sometimes leads to instabilities in the control parameters. When this happens, one generally needs larger and larger perturbations in p in order to bring the trajectory to stay inside the stable subspace. The control will eventually fail when either the required $\delta p=p-\overline{p}$ exceeds the predetermined maximum control $\delta p_{\max}$ or the value of δp becomes so large that the linear approximation in Eq. (8) is no longer valid. So and Ott proposes an idea to systematically remedy the situation [7]. (A similar approach can be found in [8].) It involves the introduction of a state-plus-parameters system, which includes the regular phase space variable $\mathbf{z}_n$ as well as all the previous variations of the parameter p according to Eq. (3).

The expanded phase space is $2m-1$ dimensional and the state vector $\mathbf{Y}_n$ assumes the form

$$\mathbf{Y}_n=\begin{pmatrix} \mathbf{z}_n \\ p_{n-m+1} \\ p_{n-m+2} \\ \vdots \\ p_{n-1} \end{pmatrix}_{(2m-1)\times 1}.$$

Based on Eq. (8), the linear dynamics around the fixed point

$$\overline{\mathbf{Y}}=\begin{pmatrix} \overline{\mathbf{z}(\overline{p})} \\ \overline{p} \\ \overline{p} \\ \vdots \\ \overline{p} \end{pmatrix}$$

is [7]

$$\mathbf{Y}_{n+1}-\overline{\mathbf{Y}}=\widetilde{\mathbf{A}}(\mathbf{Y}_n-\overline{\mathbf{Y}})+\widetilde{\mathbf{B}}(p_n-\overline{p}), \tag{12}$$

where

$$\widetilde{\mathbf{A}}=\begin{pmatrix} \mathbf{A} & \mathbf{B}^{(m)} & \mathbf{B}^{(m-1)} & \mathbf{B}^{(m-2)} & \cdots & \mathbf{B}^{(2)} \\ \mathbf{0} & 0 & 1 & 0 & \cdots & 0 \\ \mathbf{0} & 0 & 0 & 1 & \cdots & 0 \\ \vdots & \vdots & \vdots & \vdots & \vdots & \vdots \\ \mathbf{0} & 0 & 0 & 0 & \cdots & 1 \\ \mathbf{0} & 0 & 0 & 0 & \cdots & 0 \end{pmatrix}_{(2m-1)\times(2m-1)}, \tag{13}$$

with $\mathbf{0}$ an m-dimensional row vector of 0's and

$$\widetilde{\mathbf{B}}=\begin{pmatrix} \mathbf{B}^{(1)} \\ 0 \\ \vdots \\ 0 \\ 1 \end{pmatrix}_{(2m-1)\times 1}. \tag{14}$$

We note that the eigenvalues of $\mathbf{A}$ are also the eigenvalues of $\widetilde{\mathbf{A}}$ with the corresponding eigenvectors

$$\mathbf{k}_i=\begin{pmatrix} \mathbf{e}_i \\ 0 \\ \vdots \\ 0 \\ 0 \end{pmatrix},$$

$i=1,2,\ldots,m$. Clearly, the above m vectors are not enough to span the $(2m-1)$-dimensional expanded phase space. To do so one needs additional $m-1$ independent vectors. We argue that these vectors can be found in the null space of the matrix $\widetilde{\mathbf{A}}^{m-1}$. Specifically, we show in the Appendix that the subspace of the vectors $\mathbf{k}$ satisfying $\widetilde{\mathbf{A}}^{m-1}\mathbf{k}=\mathbf{0}$ is $(m-1)$ dimensional and more importantly any set of $m-1$ independent vectors denoted $\mathbf{k}_i$, $i=m+1,m+2,\ldots,2m-1$, from this space can be used together with $\mathbf{k}_i$, $i=u+1,u+2,\ldots,m$, to form the basis of the stable subspace $\mathbf{E}_s(\overline{\mathbf{Y}})$ of $\widetilde{\mathbf{A}}$.

Suppose that at time n the system trajectory falls in the neighborhood of $\overline{\mathbf{Y}}$ called the control region. To stabilize the subsequent motion around this fixed point with u unstable directions, we attempt to apply u small parametric perturbations $\delta p_n,\delta p_{n+1},\ldots,\delta p_{n+(u-1)}$ in such a way that the deviation $\delta\mathbf{Y}_{n+u}=\mathbf{Y}_{n+u}-\overline{\mathbf{Y}}$ lies entirely [7] in the stable subspace $\mathbf{E}_s(\overline{\mathbf{Y}})$. After that we set the parameter to $\overline{p}$ and the orbit approaches the fixed point under the natural dynamics. Specifically, this control can be achieved as follows. Consider the transpose of $\widetilde{\mathbf{A}}$ denoted $\widetilde{\mathbf{A}}^T$. We know that both $\widetilde{\mathbf{A}}$ and $\widetilde{\mathbf{A}}^T$ have the same eigenvalue spectrum. Furthermore, as shown in the Appendix, the contravariant unstable eigenvectors $\mathbf{v}_i$ determined by

$$\widetilde{\mathbf{A}}^T\mathbf{v}_i=\lambda_i\mathbf{v}_i \tag{15}$$

for $i=1,2,\ldots,u$ have the property that they are orthogonal to the stable subspace $\mathbf{E}_s(\overline{\mathbf{Y}})$ of $\widetilde{\mathbf{A}}$. That is, the dot products $\mathbf{v}_i^T\mathbf{k}_j=0$ for $j=u+1,u+2,\ldots,m,m+1,m+2,\ldots,2m-1$. By choosing the values of $p_n,p_{n+1},\ldots,p_{n+(u-1)}$ such that

$$\begin{aligned}\mathbf{v}_1^T\delta\mathbf{Y}_{n+u}&=0,\\ \mathbf{v}_2^T\delta\mathbf{Y}_{n+u}&=0,\\ &\vdots\\ \mathbf{v}_u^T\delta\mathbf{Y}_{n+u}&=0,\end{aligned} \tag{16}$$

we place the deviation $\delta\mathbf{Y}_{n+u}$ in the stable subspace $\mathbf{E}_s(\overline{\mathbf{Y}})$. In the Appendix we find from the equations in (16) the control law governing the parameter perturbation p_n needed at time n to be

$$p_n=\overline{p}-\left(\sum_{k=1}^{u}\frac{(\lambda_k)^u}{(\mathbf{v}_k^T\widetilde{\mathbf{B}})\prod_{i=1,i\neq k}^{u}(\lambda_k-\lambda_i)}\mathbf{v}_k^T\right)\delta\mathbf{Y}_n. \tag{17}$$

Although the values of $p_{n+1},\ldots,p_{n+u-1}$ can also be solved together with p_n at time n, the presence of system noise makes it preferable to compute p_n using Eq. (17) at every iterate n.

The contravariant vectors $\mathbf{v}_k$ are also solved explicitly. From Eq. (15), by setting arbitrarily $v_k^{(m)}=1$, we obtain the following recursive relations to determine the other components $v_k^{(i)}$ of the vector $\mathbf{v}_k$:

$$\begin{aligned}v_k^{(1)}&=a^{(m)}/\lambda_k,\\ v_k^{(2)}&=(v_k^{(1)}+a^{(m-1)})/\lambda_k,\\ v_k^{(3)}&=(v_k^{(2)}+a^{(m-2)})/\lambda_k,\\ &\vdots\\ v_k^{(m-1)}&=(v_k^{(m-2)}+a^{(2)})/\lambda_k,\\ v_k^{(m)}&=1,\\ v_k^{(m+1)}&=b^{(m)}/\lambda_k,\\ v_k^{(m+2)}&=(v_k^{(m+1)}+b^{(m-1)})/\lambda_k,\\ v_k^{(m+3)}&=(v_k^{(m+2)}+b^{(m-2)})/\lambda_k,\\ &\vdots\\ v_k^{(2m-1)}&=(v_k^{(2m-2)}+b^{(2)})/\lambda_k.\end{aligned} \tag{18}$$

[Note that the conditions in Eq. (16) imply that the lengths of the vectors $\mathbf{v}_k$ do not play a role. Thus we can set $v_k^{(m)}=1$ for simplicity.] Solving these equations we get

$$\begin{aligned}v_k^{(i)}&=\sum_{j=1}^{i}a^{(m-j+1))}/(\lambda_k)^{i-j+1},\quad i=1,2,\ldots,m-1,\\ v_k^{(m)}&=1,\\ v_k^{(i)}&=\sum_{j=1}^{i-m}b^{(m-j+1)}/(\lambda_k)^{i-m-j+1},\\ &\qquad i=m+1,m+2,\ldots,2m-1.\end{aligned} \tag{19}$$

We emphasize that all the formulas in Eqs. (17) and (19) needed for implementing the control are expressed explicitly in terms of the variables $a^{(i)}$ and $b^{(i)}$, to be estimated from the experimental time series, and the unstable eigenvalues λ_i of $\mathbf{A}$ in Eq. (10).

For fixed points with one or two unstable directions, a situation likely to be encountered in practice, the control law in Eq. (17) reduces to

$$p_n=\overline{p}-\left(\frac{\lambda_1}{(\mathbf{v}_1^T\widetilde{\mathbf{B}})}\mathbf{v}_1^T\right)\delta\mathbf{Y}_n \tag{20}$$

for $u=1$ and to

$$p_n=\overline{p}-\left(\frac{(\lambda_1)^2}{(\mathbf{v}_1^T\widetilde{\mathbf{B}})(\lambda_1-\lambda_2)}\mathbf{v}_1^T+\frac{(\lambda_2)^2}{(\mathbf{v}_2^T\widetilde{\mathbf{B}})(\lambda_2-\lambda_1)}\mathbf{v}_2^T\right)\delta\mathbf{Y}_n \tag{21}$$

for $u=2$.

C. Stabilizing a period-*N* orbit

Let a period-N orbit in the original phase space when $p=\overline{p}$ be $\overline{\mathbf{X}}_n(\overline{p}),\overline{\mathbf{X}}_{n+1}(\overline{p}),\ldots,\overline{\mathbf{X}}_{n+N}(\overline{p})=\overline{\mathbf{X}}_n(\overline{p})$. The corre-

sponding scalar time series $\{\overline{x_n(\overline{p})}\}$ is also periodic with a period of N. Suppose at time n the trajectory $\mathbf{z}_n$ in the m-dimensional reconstructed phase space comes near one of the periodic points denoted by $\bar{\mathbf{z}}_n(\overline{p})$. The entire reconstructed periodic orbit is then $\bar{\mathbf{z}}_n(\overline{p})$, $\bar{\mathbf{z}}_{n+1}(\overline{p}), \ldots, \bar{\mathbf{z}}_{n+N}(\overline{p})=\bar{\mathbf{z}}_n(\overline{p})$. The Jacobian $\mathbf{A}_n$ in Eq. (6) and the $\mathbf{B}_n$ vectors in Eq. (7) evaluated along the orbit are now functions of n, satisfying the periodic conditions $\mathbf{A}_n=\mathbf{A}_{n+N}$ and $\mathbf{B}_n^{(i)}=\mathbf{B}_{n+N}^{(i)}$. Introducing the expanded state-plus-parameters phase space, we have, close to the periodic orbit, the linear iteration equation

$$\mathbf{Y}_{n+i}-\overline{\mathbf{Y}}_{n+i}=\widetilde{\mathbf{A}}_{n+i-1}(\mathbf{Y}_{n+i-1}-\overline{\mathbf{Y}}_{n+i-1}) +\widetilde{\mathbf{B}}_{n+i-1}(p_{n+i-1}-\overline{p}), \tag{22}$$

where $i=1,2,3,\ldots$ and $\mathbf{Y}_{n+i}$, $\widetilde{\mathbf{A}}_{n+i}$, and $\widetilde{\mathbf{B}}_{n+i}$ are formed in the same way as their counterparts in Eq. (12). Assume that there are u unstable directions associated with the orbit. The control is accomplished by using u small perturbations $p_n, p_{n+1}, \ldots, p_{n+u-1}$ to place the deviation $\delta\mathbf{Y}_{n+u}=\mathbf{Y}_{n+u}-\overline{\mathbf{Y}}_{n+u}$ into the stable subspace $\mathbf{E}_s(\overline{\mathbf{Y}}_{n+u})$ of the matrix $\mathbf{J}_{n+u}=\widetilde{\mathbf{A}}_{n+u-1}\widetilde{\mathbf{A}}_{n+u-2}\cdots\widetilde{\mathbf{A}}_{n+u-N}$. Since the eigenvectors change from orbit point to orbit point the control law can no longer be expressed as explicitly as in the case of an $N=1$ fixed point. Below we give a brief description of the steps needed for arriving at the control law.

Let the unstable eigenvalues of the entire periodic orbit be $\lambda_1, \lambda_2, \ldots, \lambda_u$. The stable subspace at the orbit point $\overline{\mathbf{Y}}_{n+i}$ is determined by the matrix

$$\mathbf{J}_{n+i}=\widetilde{\mathbf{A}}_{n+i-1}\widetilde{\mathbf{A}}_{n+i-2}\cdots\widetilde{\mathbf{A}}_{n+i-N}. \tag{23}$$

As in the case of a fixed point there is no need to find this subspace explicitly for the formulation of the control law. Instead we consider the eigenvalue problem

$$\mathbf{J}_{n+i}^T\mathbf{v}_{n+i}^{(j)}=\lambda_j\mathbf{v}_{n+i}^{(j)}. \tag{24}$$

Multiplying Eq. (24) on both sides from the left by $\widetilde{\mathbf{A}}_{n+i-N-1}=\widetilde{\mathbf{A}}_{n+i-1}$ we get

$$\mathbf{J}_{n+i-1}^T\widetilde{\mathbf{A}}_{n+i-1}\mathbf{v}_{n+i}^{(j)}=\lambda_j\widetilde{\mathbf{A}}_{n+i-1}\mathbf{v}_{n+i}^{(j)}.$$

That is, the vector $\mathbf{v}_{n+i-1}^{(j)}$ is parallel to the vector $\widetilde{\mathbf{A}}_{n+i-1}^T\mathbf{v}_{n+i}^{(j)}$, namely,

$$\widetilde{\mathbf{A}}_{n+i-1}^T\mathbf{v}_{n+i}^{(j)}=c_{n+i-1}^{(j)}\mathbf{v}_{n+i-1}^{(j)}. \tag{25}$$

This definition implies the periodic condition $c_n^{(j)}=c_{n+N}^{(j)}$.

Iterating Eq. (22) u times yields

$$\begin{aligned}\delta\mathbf{Y}_{n+u}=&\widetilde{\mathbf{A}}_{n+u-1}\widetilde{\mathbf{A}}_{n+u-2}\cdots\widetilde{\mathbf{A}}_n\delta\mathbf{Y}_n\\ &+\widetilde{\mathbf{A}}_{n+u-1}\widetilde{\mathbf{A}}_{n+u-2}\cdots\widetilde{\mathbf{A}}_{n+1}\widetilde{\mathbf{B}}_n\delta p_n\\ &+\widetilde{\mathbf{A}}_{n+u-1}\widetilde{\mathbf{A}}_{n+u-2}\cdots\widetilde{\mathbf{A}}_{n+2}\widetilde{\mathbf{B}}_{n+1}\delta p_{n+1}\\ &\vdots\\ &+\widetilde{\mathbf{A}}_{n+u-1}\widetilde{\mathbf{B}}_{n+u-2}\delta p_{n+u-2}\\ &+\widetilde{\mathbf{B}}_{n+u-1}\delta p_{n+u-1}.\end{aligned}$$

Choosing the values of $\delta p_n, \delta p_{n+1}, \ldots, \delta p_{n+u-1}$ such that

$$(\mathbf{v}_{n+u}^{(j)})^T\delta\mathbf{Y}_{n+u}=0 \tag{26}$$

for $j=1,2,\ldots,u$, we place the deviation $\delta\mathbf{Y}_{n+u}$ entirely in the stable subspace $\mathbf{E}_s(\overline{\mathbf{Y}}_{n+u})$. From Eq. (26), with the aid of Eq. (25), we obtain the u equations

$$\begin{aligned}&(\mathbf{v}_n^{(j)})^T\delta\mathbf{Y}_n\prod_{k=0}^{u-1}c_{n+k}^{(j)}\\ &\quad+\sum_{i=1}^{u-1}\left((\mathbf{v}_{n+i}^{(j)})^T\widetilde{\mathbf{B}}_{n+i-1}\delta p_{n+i-1}\prod_{k=i}^{u-1}c_{n+k}^{(j)}\right)\\ &\quad+(\mathbf{v}_{n+u}^{(j)})^T\widetilde{\mathbf{B}}_{n+u-1}\delta p_{n+u-1}=0,\end{aligned} \tag{27}$$

where $j=1,2,\ldots,u$. We solve these linear equations to obtain the control law governing the parameter perturbation p_n needed at time n to be

$$p_n=\overline{p}+\frac{H}{W}, \tag{28}$$

where $W=\mathrm{Det}(\mathbf{W})$ with $w_{ij}=(\mathbf{v}_{n+j}^{(i)})^T\widetilde{\mathbf{B}}_{n+j-1}\Pi_{k=j}^{u-1}c_{n+k}^{(i)}$ and $H=\mathrm{Det}(\mathbf{H})$ with $h_{ij}=-(\mathbf{v}_u^{(i)})^T\delta\mathbf{Y}_n\Pi_{k=0}^{u-1}c_{n+k}^{(i)}$ for $j=1$ and $h_{ij}=w_{ij}$ for $j\neq 1$. Again, in order to compensate for the effect of noise in experimental applications, we recalculate at each time n the value of p_n, even though by solving the u equations in Eq. (27) simultaneously we can at once obtain parameter perturbations for the future u steps.

For the special case where the period-N orbit has one unstable direction ($u=1$), the control law takes the simple form

$$p_n=\overline{p}-\left(\frac{c_n^{(1)}(\mathbf{v}_n^{(1)})^T}{((\mathbf{v}_{n+1}^{(1)})^T\widetilde{\mathbf{B}}_n)}\right)\delta\mathbf{Y}_n. \tag{29}$$

Evidently, this equation and Eq. (20) are identical for $N=1$.

We remark that in the above we express the control laws in terms of the unstable directions of the periodic orbit. This approach offers several advantages over expressing control laws using stable directions. First, in the expanded phase space, one tends to have fewer unstable directions than stable ones that include the null space. Second, since the estimated matrix elements of **A** and **B**'s carry inevitable errors, fewer calculations reduce the chance of severe error propagations into the control law that, in turn, affect the control performance. Third, it is an empirical fact that information about unstable directions tends to be more reliably estimated from experimental time series.

III. NUMERICAL RESULTS

A. Formation of time series

In experimental problems, we expect to encounter two classes of continuous-time systems, autonomous and periodically driven. We discuss how to form discrete time series in both cases so that the control laws developed in Sec. II for discrete maps are directly applicable.

First, consider an autonomous system defined as

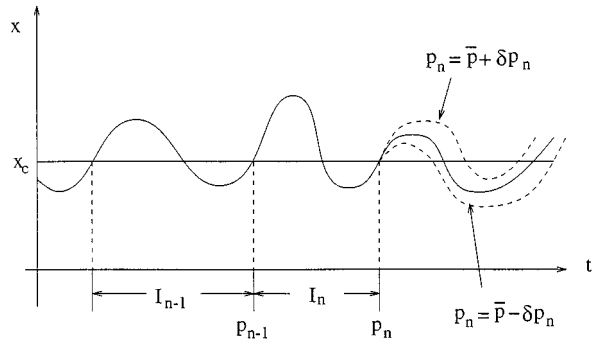

FIG. 1. Schematic illustrating the formation of interspike intervals from a continuous-time series and the effect of control on the intervals.

$$d\mathbf{Z}/dt = \mathbf{G}(\mathbf{Z},p),$$

where $\mathbf{Z} \in \mathbb{R}^{k+1}$. Let $x = h(\mathbf{Z})$ denote a scalar observable function. Consider the plot of x versus t. We form the discrete-time series by measuring the intervals I_n between the $(n-1)$th and nth upward (or downward) crossings of some predetermined threshold $x = x_c$ (see Fig. 1). We argue that these variables I_n, which we call interspike intervals, sample the dynamics of some Poincaré map in the original $\mathbf{Z}$ phase space. Specifically, at each crossing in the x versus t plot, the condition $x = h(\mathbf{Z}) = x_c$ is met. This condition defines a k-dimensional Poincaré surface of section in the original $\mathbf{Z}$ space. Thus I_n is also the time between the $(n-1)$th and the nth crossings of the section. Suppose we parametrize this section by a k-dimensional vector $\mathbf{Q}$. Then, the successive crossings of the plane from a given direction by a chaotic trajectory give rise to a Poincaré map

$$\mathbf{Q}_{n+1} = \mathbf{P}(\mathbf{Q}_n, p). \tag{30}$$

Realizing that the interval I_n is uniquely determined by $\mathbf{Q}_{n-1}$, namely,

$$I_n = \Phi(\mathbf{Q}_{n-1}), \tag{31}$$

we complete the analogy between Eqs. (30) and (1) and the analogy between Eqs. (31) and (2).

Traditionally, one measures the continuous-time series x versus t using equally spaced sampling intervals. In the reconstructed phase space one obtains the Poincaré map by examining the crossings of some plane by the reconstructed trajectory. Due to the discreteness of the trajectory one introduces inevitable errors in the resulting Poincaré map through interpolation. In contrast, our way of forming the discrete time series using interspike intervals avoids this problem by monitoring the analog signal and thus detecting the threshold crossing precisely. Furthermore, the reconstructed interspike intervals already obey a Poincaré map. In Fig. 1 we also illustrate the effect of parametric perturbations on the interspike intervals.

Next, we consider a periodically forced system

$$d\mathbf{Z}/dt = \mathbf{G}(\mathbf{Z},t,p),$$

where $\mathbf{Z} \in \mathbb{R}^k$ and $\mathbf{G}(\mathbf{Z},t+T,p) = \mathbf{G}(\mathbf{Z},t,p)$. Let $x = h(\mathbf{Z})$ be the scalar observable function. Since by introducing t as an additional variable one can convert a nonautononmous system to an autononmous one, the interspike intervals formation method also applies here. Another more traditional method of forming a discrete-time series $\{x_n\}$ is by measuring x at times $t_n = nT + T_0$ (stroboscopic sampling). From the theorems of [12], the dynamics reconstructed from $\{x_n\}$ in a suitable delay coordinates space represents the dynamics of the Poincaré map $\mathbf{Z}_{n+1} = \mathbf{P}(\mathbf{Z}_n)$ in the original phase space, which, in turn, is equivalent to the continuous-time dynamics described by the differential equations. Below we give two examples of controlling continuous-time chaotic systems using the methods above.

B. Control example 1

Consider the following five-dimensional system of two coupled driven Duffing oscillators:

$$\begin{aligned} \ddot{x}_1 + \gamma\dot{x}_1 + \alpha(x_1^3 - x_1) + \beta_1(x_1 - x_2) &= p_1 \sin(\omega t), \\ \ddot{x}_2 + \gamma\dot{x}_2 + \alpha(x_2^3 - x_2) + \beta_2(x_2 - x_1) &= p \sin(\omega t). \end{aligned} \tag{32}$$

For $\gamma = 0.632$, $\alpha = 4.0$, $\beta_1 = 0.1$, $\beta_2 = 0.05$, $\omega = 2.1235$, $p_1 = 1.011$, and $p = \overline{p} = p_1$, Eq. (32) exhibits a chaotic attractor of dimension $D = 3.3$. The scalar observable here is $x = x_1 + x_2$ and we sample the attractor every cycle of the external forcing. The attractor reconstructed using the time series $\{x_n\}$ in an $(m = 4)$-dimensional delay coordinates space has a dimension $D = 2.3$. Figure 2(a) shows the attractor projected down to a two-dimensional space. The high-dimensional character of this attractor is apparent.

The reconstructed attractor contains a fixed point $(N = 1)$ at $\bar{\mathbf{z}}(\overline{p}) = (0.54, 0.54, 0.54, 0.54)^T$ with two unstable directions $(u = 2)$. This fixed point corresponds to the synchronized period-1 motion of the coupled oscillators. Our objective is to stabilize this motion. From numerically generated time series we estimate a_i and b_i used in the $\mathbf{A}$ matrix and the $\mathbf{B}$ vectors to be approximately $a^{(1)} = -3.05$, $a^{(2)} = -2.23$, $a^{(3)} = 0.0$, $a^{(4)} = 0.016$ and $b^{(1)} = -0.90$, $b^{(2)} = -0.089$, $b^{(3)} = 0.78$, $b^{(4)} = -0.056$. The two unstable eigenvalues are $\lambda_1 = -1.85$ and $\lambda_2 = -1.20$. Applying the control law in Eq. (17), we stabilize the fixed point as shown in Fig. 2(b), which displays the behavior of the system before and after the control is turned on.

C. Control example 2

Consider the four-dimensional autonomous chemical reaction model [13]

$$\begin{aligned} \dot{x} &= pw/(1 + w^{10}) - 0.1x, \\ \dot{y} &= 0.1x - 0.2yz, \\ \dot{z} &= 0.2z(y - w), \\ \dot{w} &= 0.2zw - 0.1w. \end{aligned} \tag{33}$$

For $p = \overline{p} = 2.5$ this system exhibits a chaotic attractor of dimension $D = 2.2$. Assume that the observed scalar variable is x itself. By measuring the times between successive upward crossings of some threshold x_c by the x versus t function we form the interspike interval time series $\{I_n\}$. Reconstructing

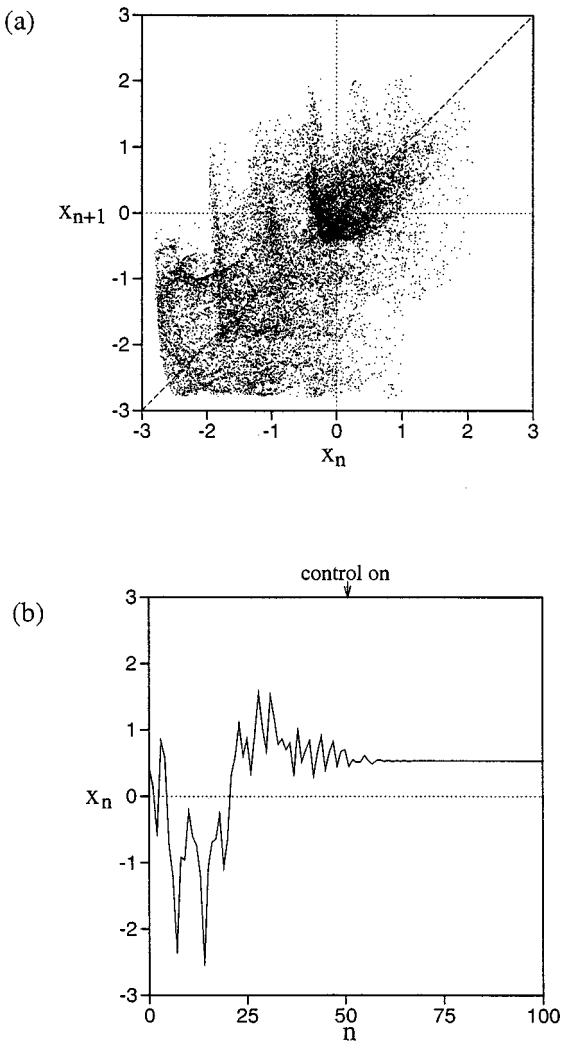

FIG. 2. (a) Two-dimensional ($m=2$) reconstructed image of the attractor from the coupled Duffing equations, Eq. (32). High-dimensional nature of the dynamics is apparent. (b) The result of applying an $m=4$ implementation of our control method. Here discrete stroboscopic samples are connected with straight lines.

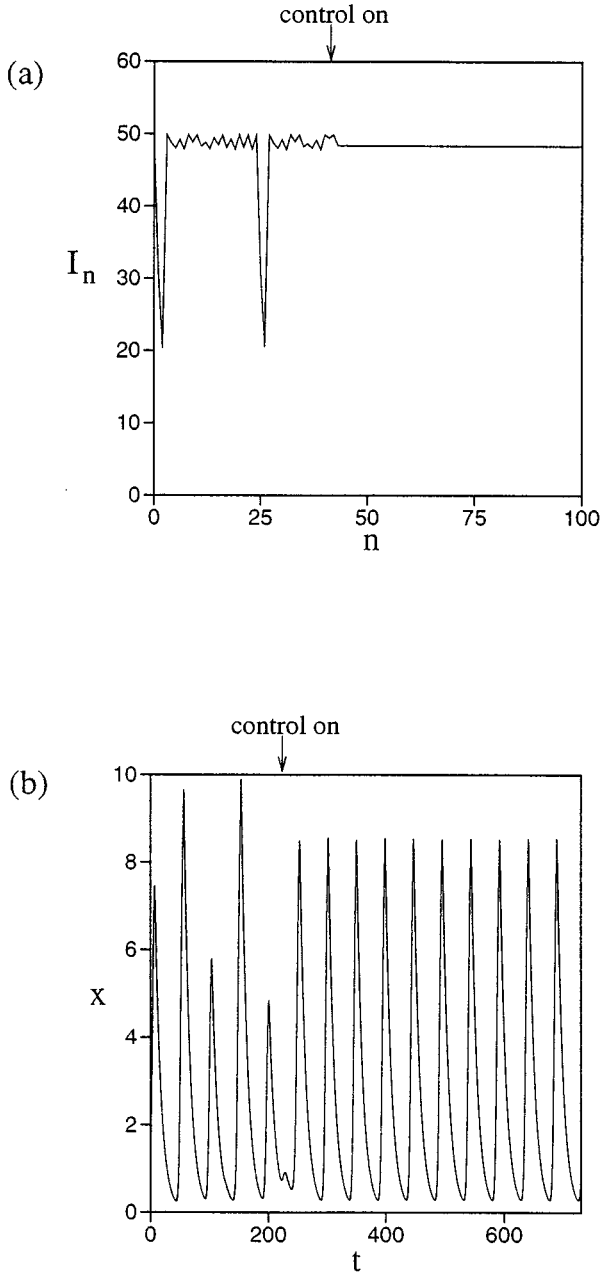

FIG. 3. Results of controlling the unstable period-1 orbit in the chemical reaction model Eq. (33) using an $m=3$ implementation of the control. (a) The interspike intervals and (b) the corresponding continuous-time series.

this discrete time series in an $(m=3)$-dimensional delay coordinate space we obtain an attractor of dimension 1.2. In this attractor there is a fixed point $(N=1)$ at $\mathbf{z}_n=(48.40,48.40,48.40)^T$ and a period-2 orbit $(N=2)$ cycling between $\overline{\mathbf{z}_1(p)}=(47.74,50.13,47.74)^T$ and $\overline{\mathbf{z}_2(p)}=(50.13,47.74,50.13)^T$. Both orbits are found to have one unstable direction $(u=1)$.

First, consider the control of the fixed point. Set $x_c=1$. From the numerically generated time series we obtain $a^{(1)}=-1.33$, $a^{(2)}=0.41$, $a^{(3)}=-0.008$ and $b^{(1)}=-1.25$, $b^{(2)}=-3.20$, $b^{(3)}=1.95$. The unstable eigenvalue is calculated to be $\lambda_1=-1.59$. The result of applying Eq. (20) is shown in Fig. 3, where the system behavior before and after the control is turned on is displayed. Figure 3(a) is the interspike intervals and Fig. 3(b) gives the corresponding continuous time series.

Next, consider the control of the period-2 orbit. Set $x_c=3$. From the time series we estimate the elements of the **A** matrix and the **B** vectors at $\mathbf{z}_1(\overline{p})$ to be $a^{(1)}=-1.56$, $a^{(2)}=0.042$, $a^{(3)}=6.0\times10^{-5}$, and $b^{(1)}=1.81$, $b^{(2)}=-3.32$, $b^{(3)}=1.61$ and at $\mathbf{z}_2(\overline{p})$ to be $a^{(1)}=2.15$, $a^{(2)}=0.15$, $a^{(3)}=2.9\times10^{-3}$ and $b^{(1)}=-2.79$, $b^{(2)}=5.85$, $b^{(3)}=0.17$. The control law in Eq. (29) is completely determined by these values. In Fig. 4 we show the result of control by displaying the interspike intervals (a) and the corresponding continuous time series (b) for before and after the control is activated.

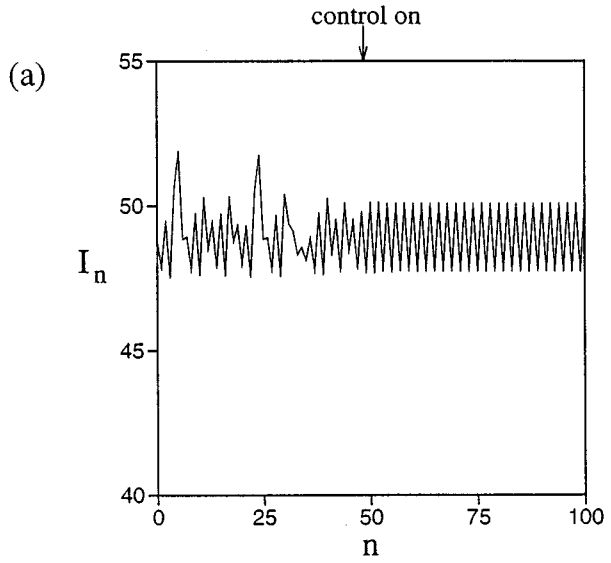

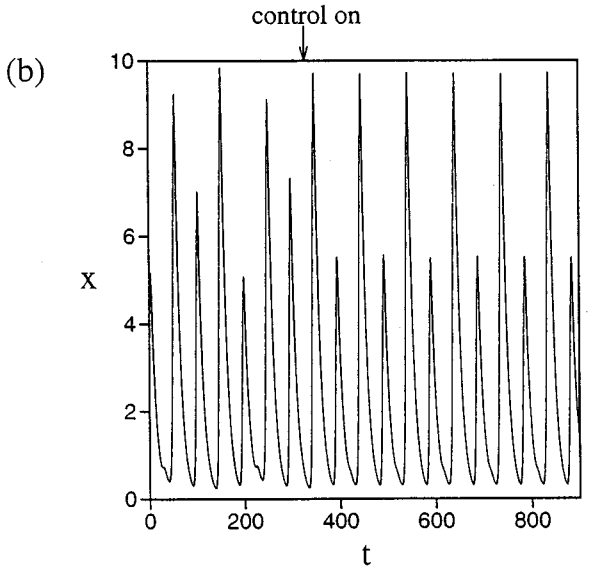

FIG. 4. Results of controlling the unstable period-2 orbit in the chemical reaction model Eq. (33) using an $m=3$ implementation of the control. (a) The interspike intervals and (b) the corresponding continuous-time series.

IV. EXPERIMENTAL RESULTS

A. Setup

Our experimental system consists of a magnetoelastic metal ribbon clamped at its lower end. The ribbon changes its Young's modulus by more than a factor of 10 in response to an external magnetic field and buckles under gravity as a result. This highly nonlinear system is placed vertically within three mutually orthogonal pairs of Helmholtz coils. The two horizontal pairs of the Helmholtz coils are used for counteracting the Earth's magnetic field while the vertical pair is used to supply an approximately uniform field along the ribbon's length. Inside the Helmholtz coils a photonic sensor is used to measure the ribbon's position at a given point. This sensor is mounted a short distance above the base of the ribbon. To obtain chaos, we drive the ribbon with a time-varing magnetic field in the form $H(t)=H_{\rm dc}+H_{\rm ac}\sin(2\pi ft)$, which is applied along the vertical direction. For $f=1.03$ Hz, $H_{\rm ac}=0.961$ Oe, and $H_{\rm dc}=\overline{H}_{\rm dc}=-1.350$ Oe the ribbon exhibits chaotic oscillations. We choose $p=H_{\rm dc}$ as the control parameter.

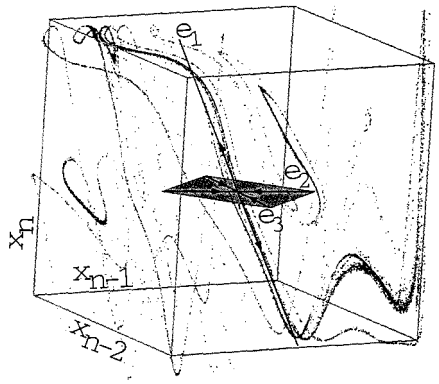

FIG. 5. Time series from the magnetoelastic ribbon reconstructed in a three-dimensional ($m=3$) delay coordinate space. The local dynamics near the fixed point is described by one unstable ($\mathbf{e}_1$) and two stable directions ($\mathbf{e}_2$ and $\mathbf{e}_3$).

Denote the position of the ribbon measured by the photonic sensor every driving period as x_n. From visual inspections of the reconstructed attractor in the $m=2$ space and from some simple estimates it is apparent that the dynamical behavior near the fixed point, which we wish to stabilize, cannot be effectively characterized by one stable direction and one unstable direction. High-dimensional embedding spaces are needed to unfold the local dynamics in this case. This observation is further confirmed by our inability to bring about the desired control using the original Ott-Grebogi-Yorke (OGY) method [2] (see below) as well as using the $m=2$ implementation of our control method, which incorporates the effect of delay coordinates and is equivalent to the Dressler and Nitsche's method [6].

Next we reconstruct the time series in an $(m=3)$-dimensional space as shown in Fig. 5. On the chaotic attractor we identify an unstable periodic orbit of period-1 by looking for saddle points lying on the diagonal. From the experimental data this fixed point is determined to be $\overline{\mathbf{z}}(\overline{p})=(6.35, 6.35, 6.35)^T$. To stabilize the system around this unstable fixed point, we choose $p=H_{\rm dc}$ as the control parameter. When the system state point falls in the vicinity of the unstable fixed point, a small time-dependent change was made to this parameter such that the next iterate would fall onto the stable plane defined by the two stable eigenvectors. The perturbation size is calculated according to Eq. (20). To determine the matrix elements $a^{(1)}$, $a^{(2)}$, and $a^{(3)}$ for $\mathbf{A}$ in Eq. (10) we consider a close return event by choosing a point in the close vicinity of the fixed point and finding its preimage and two future iterates. The reason for using the preimage is to better represent the stable directions and the reason for using two future iterates instead of just one is to pick up the negative sign often associated with the unstable eigenvalue. To guard against the detection of a false

nearest neighbor in a three-dimensional embedding space we also monitor the delay coordinate map in the $m=4$ and $m=5$ space. From the true nearest-neighbor points we do a least-squares fit to determine $a^{(1)}$, $a^{(2)}$, and $a^{(3)}$ to a high accuracy. Using 20 close return events we find $a^{(1)}=-1.033\,68$, $a^{(2)}=1.7890$, and $a^{(3)}=0.0935$, respectively. From the matrix the unstable eigenvalue was calculated to be $\lambda_1=-1.9338$. The values of $b^{(1)}$, $b^{(2)}$, and $b^{(3)}$ are calculated from the experimental data when a perturbation p_n is applied at time n immediately after a point in the map comes into the vicinity of the unstable fixed point. The perturbation lasts for the full duration of the drive period. When the future section data are measured at time $n+1$, $n+2$, and $n+3$, we calculate the coefficients $b^{(1)}$, $b^{(2)}$, and $b^{(3)}$ according to

$$b^{(1)}=\frac{\delta x_{n+1}-a^{(1)}\delta x_n-a^{(2)}\delta x_{n-1}-a^{(3)}\delta x_{n-2}}{\delta p_n},$$

$$b^{(2)}=\frac{\delta x_{n+2}-a^{(1)}\delta x_{n+1}-a^{(2)}\delta x_n-a^{(3)}\delta x_{n-1}}{\delta p_n},$$

$$b^{(3)}=\frac{\delta x_{n+3}-a^{(1)}\delta x_{n+2}-a^{(2)}\delta x_{n+1}-a^{(3)}\delta x_n}{\delta p_n}.$$

In the experiment we use a constant $\delta p_n=0.038$ Oe every time for perturbation. For a typical run in this experiment the values of $b^{(1)}$, $b^{(2)}$, and $b^{(3)}$ are determined to be 0.001 23 V/Oe, $-0.000\,118$ V/Oe, and $-0.000\,414$ V/Oe, respectively.

B. Results

Using the $m=3$ implementation of our control method with the estimated $a^{(i)}$'s and $b^{(i)}$'s as stated above, we have successfully controlled the chaotic oscillations of the ribbon for almost 200 000 driving cycles (about 54 h) without any loss of control. Figure 6(a) shows a portion of the experimental time series before and after the application of control. The control can be maintained indefinitely. Figure 6(b) shows the perturbations applied to stabilize the period-1 orbit. Notice that the size of the perturbations is very small, typically between ± 0.0054 Oe, or about 0.4% of the nominal dc field $\overline{p}=H_{\rm dc}$. Figure 7(a) shows the contrast between the original OGY control [2] and our high-dimensional control with $m=3$ on the same attractor. After 830 iterates the OGY control is turned on and is unable to hold the periodic orbit even though there are numerous attempts on the close returns. The perturbed orbits would come in along the stable direction, but once the orbit reaches the unstable fixed point it starts to depart from the vicinity of the fixed point. In contrast, when our high-dimensional control is activated the system is captured into the period-1 motion rapidly. We note that the $m=2$ implementation of our method, which has the delay coordinates effect taken into account, also failed to achieve proper control. This leads us to believe that for this attractor one needs a higher-dimensional embedding space to unfold the dynamics and implement control.

We have also studied another parameter setting where the local dynamics near the fixed point can be effectively described by one stable and one unstable direction. We are able

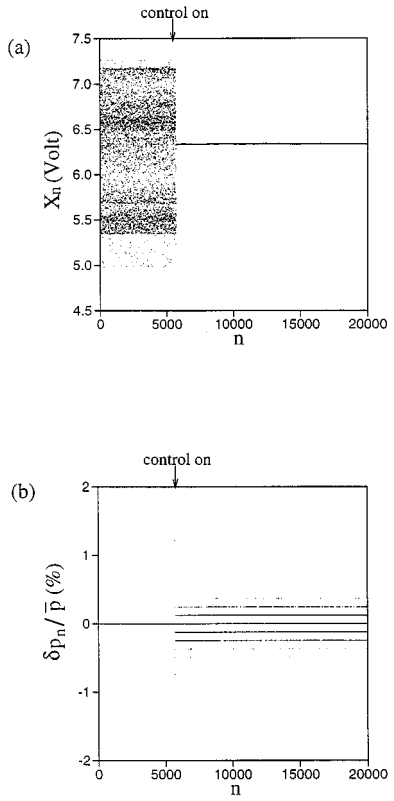

FIG. 6. Results of stabilizing the unstable period-1 orbit using an $m=3$ implementation of our control method. (a) Time series and (b) parameter perturbations. We note that the magnitude of δp_n is about 0.4% of the nominal value of $\overline{p}$, where $p=H_{\rm dc}$ is the dc field.

to control the period-1 orbit in this case with the original OGY method [2]. However, the interesting point is that, by applying the $m=3$ implementation of our method to the same orbit, we are able to achieve control with smaller parameter perturbations compared to the OGY case. This indicates that in some situations, although the low-dimensional control is effective, a higher-dimensional implementation may prove to be more efficient. Details of this result are planned to be presented in a future paper where we consider all the practical aspects of our control technique.

In applications, an important question is the impact of noise on the control performance. The unperturbed ribbon system has about 5% intrinsic noise. Our method is unaffected by this amount of noise. To test the method further, we have also added parametric noise to the system and found that we are able to maintain control even in the presence of about 10% of additional parametric noise, demonstrating the method's robustness. We thus believe that the technique presented in the paper is viable in practical problems where chaos control in high-dimensions is desired. Again we wish to present more detailed results on the issue of noise in a future paper.

V. CONCLUSION

Since Ott, Grebogi, and Yorke published their seminal paper on the control of chaos [2], a great deal of experimental research in nonlinear dynamics has been dedicated to the exploration of various aspects of the OGY algorithm in a

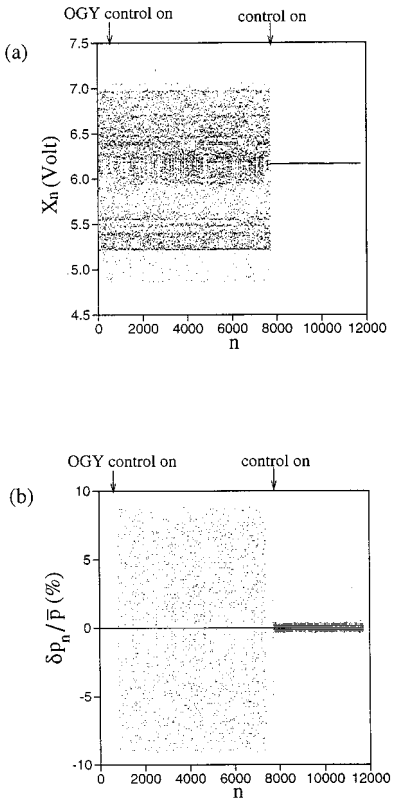

FIG. 7. Comparison of the OGY control and the $m=3$ implementation of our control method. (a) Time series and (b) parameter perturbations.

variety of systems. However, the success of the original OGY theory is limited by the fact that it applies only to systems where the dynamics near the periodic orbit is adequately described by one stable and one unstable direction. In the past few years a number of high-dimensional algorithms have been proposed to address this problem [7–9]. Due to the difficulties in obtaining the coefficients needed for control and sensitivity to noise, these methods are found to be difficult to implement experimentally.

Our main contribution in this paper is the development of a high-dimensional chaos control method that is effective and easy to implement in experiments. Based on the use of time series and delay coordinates, the method requires only small perturbations of a single control parameter to stabilize a periodic orbit in an arbitrary dimensional delay coordinate embedding space with an arbitrary number of unstable directions. In addition, by considering map-based systems our method offers the advantage that the coefficients needed for experimental implementation are easily and reliably estimated from time series data. In this regard, simple methods are proposed to extract such map-based time series from continuous-time systems. The effectiveness of the control method is demonstrated when applied to two examples of ordinary differential equations and to a physical experiment of a magnetoelastic ribbon driven by a sinusoidally varying magnetic field. Robust control is achieved in all cases. Furthermore, we mention that the method is not sensitive to noise and works well even in the presence of substantial noise.

ACKNOWLEDGMENTS

M.D. gratefully acknowledges support from the Office of Naval Research. W.L.D. is supported by the ONR Young Investigator Program. M.L.S. gratefully acknowledges support from the NSWC Independent Research Program and from the Office of Naval Research (Division of Physics and Chemistry).

APPENDIX

1. The null space of $\tilde{\mathbf{A}}^{m-1}$

Using matrix blocks we rewrite $\tilde{\mathbf{A}}$ defined in Eq. (13) as

$$\tilde{\mathbf{A}}=\begin{pmatrix} \mathbf{A} & \mathbf{B} \\ \mathbf{Z}_0 & \mathbf{S} \end{pmatrix},$$

where $\mathbf{B}$ is an $m\times(m-1)$ matrix with $\mathbf{B}^{(i)}$ its column vectors, $\mathbf{Z_0}$ is an $(m-1)\times m$ zero matrix, and

$$\mathbf{S}=\begin{pmatrix} 0 & 1 & 0 & \cdots & 0 \\ 0 & 0 & 1 & \cdots & 0 \\ \vdots & \vdots & \vdots & \vdots & \vdots \\ 0 & 0 & 0 & \cdots & 1 \\ 0 & 0 & 0 & 0 & 0 \end{pmatrix}_{(m-1)\times(m-1)} .$$

It is easy to verify that $\mathbf{S}^{m-1}$ is a matrix of zeros. This means that the eigenvalue problem $\tilde{\mathbf{A}}^{m-1}\mathbf{k}=\mathbf{0}$ has m equations for $2m-1$ unknowns from which one can find $m-1$ independent basis vectors to span the null vector $\mathbf{k}$. In other words, the null space of $\tilde{\mathbf{A}}^{m-1}$ is $(m-1)$ dimensional.

2. The unstable eigenvectors of $\tilde{\mathbf{A}}^{T}$

We wish to show that $\mathbf{v}_i$ from $\tilde{\mathbf{A}}^T\mathbf{v}_i=\lambda_i\mathbf{v}_i$, $i=1,2,\ldots,u$, is orthogonal to the stable subspace spanned by $\mathbf{k}_j$, $j=u+1,u=2,\ldots,2m-1$. Consider $j=u+1,u+2,\ldots,m$. Multiply Eq. (15) from both sides by $\mathbf{k}_j^T$. The left-hand side becomes $\mathbf{k}_j^T\tilde{\mathbf{A}}^T\mathbf{v}_i=(\tilde{\mathbf{A}}\mathbf{k}_j)^T\mathbf{v}_i=\lambda_j\mathbf{k}_j^T\mathbf{v}_i$. Equating it with the right-hand side $\lambda_i\mathbf{k}_j^T\mathbf{v}_i$ and using $\lambda_i\neq\lambda_j$ we have $\mathbf{k}_j^T\mathbf{v}_i=\mathbf{v}_i^T\mathbf{k}_j=0$. Similarly, one can show that $\mathbf{v}_i^T\mathbf{k}_j=0$, $j=m+1,m+2,\ldots,2m-1$, by considering the eigenvalue problem of $\tilde{\mathbf{A}}^{m-1}$ instead of $\tilde{\mathbf{A}}$. It is straightforward to see that if the deviation $\delta\mathbf{Y}_{n+u}$ lies entirely in the space of $\mathbf{k}_j$, $j=u+1,u+2,\ldots,m,m+1,m+2,\ldots,2m-1$, then its future evolution asymptotically approaches zero under repeated applications of $\tilde{\mathbf{A}}$.

3. The derivation of the control law Eq. (17) from Eq. (16)

Iterating Eq. (12) u times yields

$$\delta\mathbf{Y}_{n+u}=\tilde{\mathbf{A}}^u\delta\mathbf{Y}_n+\tilde{\mathbf{A}}^{u-1}\tilde{\mathbf{B}}\delta p_n+\tilde{\mathbf{A}}^{u-2}\tilde{\mathbf{B}}\delta p_{n+1}+\cdots+\tilde{\mathbf{B}}\delta p_{n+u-1}.$$

From Eq. (16) we get

$$\lambda_1^{u-1}\delta p_n+\lambda_1^{u-2}\delta p_{n+1}+\cdots+\delta p_{n+u-1}=-\left(\frac{\lambda_1^u\mathbf{v}_1^T}{(\mathbf{v}_1^T\widetilde{\mathbf{B}})}\right)\delta\mathbf{Y}_n,$$

$$\lambda_2^{u-1}\delta p_n+\lambda_2^{u-2}\delta p_{n+1}+\cdots+\delta p_{n+u-1}=-\left(\frac{\lambda_2^u\mathbf{v}_2^T}{(\mathbf{v}_2^T\widetilde{\mathbf{B}})}\right)\delta\mathbf{Y}_n,$$

$$\vdots$$

$$\lambda_u^{u-1}\delta p_n+\lambda_u^{u-2}\delta p_{n+1}+\cdots+\delta p_{n+u-1}=-\left(\frac{\lambda_u^u\mathbf{v}_u^T}{(\mathbf{v}_u^T\widetilde{\mathbf{B}})}\right)\delta\mathbf{Y}_n.$$

These u linear equations contain u unknowns. Using Cramer's rule we express p_n as

$$p_n=\overline{p}+\frac{C}{D},$$

where

$$C=\mathrm{Det}\begin{pmatrix} -[\lambda_1^u\mathbf{v}_1^T/(\mathbf{v}_1^T\widetilde{\mathbf{B}})]\delta\mathbf{Y}_n & \lambda_1^{u-2} & \lambda_1^{u-3} & \cdots & 1 \\ -[\lambda_2^u\mathbf{v}_2^T/(\mathbf{v}_2^T\widetilde{\mathbf{B}})]\delta\mathbf{Y}_n & \lambda_2^{u-2} & \lambda_2^{u-3} & \cdots & 1 \\ \vdots & \vdots & \vdots & \vdots & \vdots \\ -[\lambda_u^u\mathbf{v}_u^T/(\mathbf{v}_u^T\widetilde{\mathbf{B}})]\delta\mathbf{Y}_n & \lambda_u^{u-2} & \lambda_u^{u-3} & \cdots & 1 \end{pmatrix}_{u\times u} \tag{A1}$$

and

$$D=\mathrm{Det}\begin{pmatrix} \lambda_1^{u-1} & \lambda_1^{u-2} & \lambda_1^{u-3} & \cdots & 1 \\ \lambda_2^{u-1} & \lambda_2^{u-2} & \lambda_2^{u-3} & \cdots & 1 \\ \vdots & \vdots & \vdots & \vdots & \vdots \\ \lambda_u^{u-1} & \lambda_u^{u-2} & \lambda_u^{u-3} & \cdots & 1 \end{pmatrix}_{u\times u}. \tag{A2}$$

By recognizing that D in (A2) is a slight variant of the standard Vandermonde determinant [14] we find

$$D=(-1)^{(d^2-d)/2}\prod_{1\leqslant i<j\leqslant u}(\lambda_j-\lambda_i).$$

Expanding the determinant in Eq. (A1) about the first column, the resulting cofactors are again variants of the Vandermonde matrix. This leads us to

$$C=\sum_{k=1}^{u}(-1)^{k+(d^2-3d+2)/2}[\lambda_k^u\mathbf{v}_k^T/(\mathbf{v}_k^T\widetilde{\mathbf{B}})]\delta\mathbf{Y}_n \times\prod_{1\leqslant i<j\leqslant u,i\neq k,j\neq k}(\lambda_j-\lambda_i).$$

After some algebra we obtain Eq. (17).

[1] E. Ott, *Chaos in Dynamical Systems* (Cambridge University Press, Cambridge, 1993).

[2] E. Ott, C. Grebogi, and J.A. Yorke, Phys. Rev. Lett. **64**, 1996 (1990).

[3] W.L. Ditto, S.N. Rauseo, and M.L. Spano, Phys. Rev. Lett. **65**, 3211 (1990); E.R. Hunt, *ibid.* **67**, 1953 (1991); R. Roy, T.W. Murphy, T.D. Maier, Z. Gills, and E.R. Hunt, *ibid* **68**, 1259 (1992); A. Garfinkel, M.L. Spano, W.L. Ditto, and J.N. Weiss, Science **257**, 1230 (1992); V. Petrov, V. Caspar, J. Masere, and K. Showalter, Nature (London) **361**, 240 (1993); S.J. Schiff, K. Jerger, D.H. Duong, T. Chang, M.L. Spano, and W.L. Ditto, *ibid.* **370**, 615 (1994); J.E.S. Socolar, D.W. Sukow, and D.J. Gauthier, Phys. Rev. E **50**, 3245 (2994); P. Parmananda, M.A. Rhode, G.A. Johnson, R.W. Rollins, H.D. Dewald, and A.J. Markworth, *ibid.* **49**, 5007 (1994).

[4] E.A. Jackson and A. Hubler, Physica D **44**, 407 (1990); B. Peng, V. Petrov, and K. Showalter, J. Phys. Chem. **95**, 4957 (1991); T. Tel, J. Phys. A **24**, L1359 (1991); K. Pyragas, Phys. Lett. A **170**, 421 (1992); Y.-C. Lai, M. Ding, and C. Grebogi, Phys. Rev. E **47**, 86 (1993); M.A. Matias and J. Guemez, Phys. Rev. Lett. **72**, 1455 (1994); M. Ding, E. Ott, and C. Grebogi, Physica D **74**, 386 (1994); D. Vassiliadis, *ibid.* **71**, 319 (1994); D.J. Christini and J.J. Collins, Phys. Rev. E (to be published).

[5] For reviews, see T.A. Shinbrot, C. Grebogi, E. Ott, and J.A. Yorke, Nature (London) **363**, 411 (1993); W.L. Ditto and L. Pecora, Sci. Am. **269** (8), 78 (1993); G. Chen and X. Dong, Int. J. Bif. Chaos **3**, 1363 (1993); E.R. Hunt and G. Johnson, IEEE Spectrum **30** (11), 32 (1993); R. Roy, Z. Gills, and K.S. Thornburg, Opt. Photon. News **5** (5), 8 (1994); E. Ott and M.L. Spano, Phys. Today **48** (5) 34 (1995).

[6] U. Dressler and G. Nitsche, Phys. Rev. Lett. **68**, 1 (1992); G. Nitsche and U. Dressler, Physica D **58**, 153 (1992).

[7] P. So and E. Ott, Phys. Rev. E **51**, 2955 (1995).

[8] V. Petrov, E. Mihaliuk, S.K. Scott, and K. Showalter, Phys. Rev. E **51**, 3988 (1995).

[9] For a sample of works dealing with chaos control in high dimensions, see F.J. Romeiras, C. Grebogi, E. Ott, and W.P. Dayawansa, Physica D **58**, 165 (1992); D. Auerbach, C. Grebogi, E. Ott, and J.A. Yorke, Phys. Rev. Lett. **69**, 3479 (1992); J.A. Sepulchre and A. Babloyantz, Phys. Rev. E **48**, 945 (1993); G. Hu and K. He, Phys. Rev. Lett. **71**, 3794 (1993); C. Reyl, L. Flepp, R. Badii, and E. Brun, Phys. Rev. E 47, 267 (1993); P. Colet, R. Roy, and K. Wiesenfeld, *ibid.* **50**, 3453 (1994); G. Hu and Z. Qu, Phys. Rev. Lett. **72**, 68 (1994); I.B. Schwartz and I. Triandaf, Phys. Rev. E **50**, 2548 (1994); A. Namajunas, K. Pyragas, and A. Tamasevicius, Phys. Lett. A **204**, 255 (1995).

[10] Edward Ott (private communication).

[11] J.-P. Eckmann and D. Ruelle, Rev. Mod. Phys. **57**, 617 (1985).

[12] F. Takens, in *Dynamical Systems and Turbulence*, edited by D. Rand and L.S. Young (Springer-Verlag, Berlin, 1981), p. 366; T. Sauer, J.A. Yorke, and M. Casdagli, J. Stat. Phys. **65**, 579 (1991).

[13] G. Baier and S. Sahle, J. Chem. Phys. **100**, 8907 (1994).

[14] R. Bellman, *Introduction to Matrix Analysis* (McGraw-Hill, New York, 1970).